

Femtosecond Time-Delay X-ray Holography

Henry N. Chapman^{1,2}, Stefan P. Hau-Riege¹, Michael J. Bogan¹, Saša Bajt¹, Anton Barty¹, Sébastien Boutet^{1,3,4}, Stefano Marchesini^{1†}, Matthias Frank¹, Bruce W. Woods¹, W. Henry Benner¹, Richard A. London¹, Urs Rohner¹, Abraham Szöke¹, Eberhard Spiller¹, Thomas Möller⁵, Christoph Bostedt⁵, David A. Shapiro^{2†}, Marion Kuhlmann⁶, Rolf Treusch⁶, Elke Plönjes⁶, Florian Burmeister⁴, Magnus Bergh⁴, Carl Caleman⁴, Gösta Huldt⁴, M. Marvin Seibert⁴ & Janos Hajdu^{3,4}.

1. University of California, Lawrence Livermore National Laboratory, 7000 East Avenue, Livermore CA 94550, USA.

2. Center for Biophotonics Science and Technology, University of California, Davis, 2700 Stockton Blvd., Suite 1400, Sacramento, CA 95817, USA.

3. Stanford Synchrotron Radiation Laboratory, Stanford Linear Accelerator Center, 2575 Sand Hill Road, Menlo Park, California 94305, USA.

4. Laboratory of Molecular Biophysics, Department of Cell and Molecular Biology, Uppsala University, Husargatan 3, Box 596, SE-75124 Uppsala, Sweden.

5. Institut für Optik und Atomare Physik, Technische Universität Berlin, Hardenbergstraße 36, PN 3-1, 10623 Berlin, Germany.

6. Deutsches Elektronen-Synchrotron, DESY, Notkestraße 85, D-22607 Hamburg, Germany.

[†] Current address: Advanced Light Source, Lawrence Berkeley National Laboratory, Berkeley, CA 94720, USA.

Extremely intense and ultrafast X-ray pulses from free-electron lasers offer unique opportunities to study fundamental aspects of complex transient phenomena in materials. Ultrafast time-resolved methods usually require highly synchronized pulses to initiate a transition and then probe it at a precisely defined time delay. In the X-ray regime, these methods are challenging since they require complex optical systems and diagnostics. Here we propose and apply a simple holographic measurement scheme, inspired by Newton’s “dusty mirror” experiment¹ to monitor the X-ray induced explosion of microscopic objects. The sample is placed near an X-ray mirror, and after the pulse traverses the sample, triggering the reaction, it is reflected back on to the sample by the mirror to probe this reaction. The delay is encoded in the resulting diffraction pattern to an accuracy of 1 fs, and the sample depth is holographically recorded to sub-wavelength accuracy. We apply the technique to monitor the dynamics of polystyrene spheres in intense FEL pulses, and observe an explosion occurring well after the initial pulse. Our results support the notion that X-ray flash imaging^{2,3} can be used to achieve high resolution, beyond radiation damage limits for biological samples⁴. With upcoming ultrafast X-ray sources we will be able to explore the three-dimensional dynamics of materials at interatomic lengthscales at the timescale of atomic motion.

One of the earliest recorded observations of interference was made by Newton¹ in the “dusty mirror” experiment. In a darkened room, Newton used a prism and a small hole in a screen to form a quasi-monochromatic beam from sunlight, which he shone onto a back-quicksilvered mirror. The mirror was angled to return the beam back through the hole, and on the screen Newton observed dark and light rings of light, which he found “strange and surprising”. Newton determined that the squares of the diameters of the bright rings followed an integer progression and the diameters depended on the thickness of the glass; a front-surface metal mirror did not produce

these rings. The ring phenomenon was later explained by Young⁵ as being caused by the interference at the screen between two paths of light scattering from dust particles on the mirror's front surface: on one path the light scatters from a particle on its way in towards the mirror, after which it reflects from the silvered surface, and on the other, the light is first reflected from the silvered surface before scattering from this same particle only after emerging from the glass. Such "diffusion rings" as they were known can be seen with white light and were a common bane of optical instruments well into the twentieth century, until the use of vacuum coatings⁶.

Our experiment makes use of Newton's geometry to follow the X-ray induced explosion of uniform polystyrene spheres in a FEL pulse, using a focused 25 fs pulse of 32.5-nm wavelength light from the FLASH soft-X-ray laser⁷. We placed 140-nm diameter spherical polystyrene particles on a 20-nm thick silicon nitride membrane that was mounted with a thin spacer in front of a multilayer mirror, this assembly resembling Newton's dusty mirror. Instead of a screen we used another plane mirror angled at 45° to reflect the interference pattern onto a back-illuminated CCD detector, as shown in Fig. 1. Some interference patterns, recorded with single pulses of about 1.6×10^{12} photons (or 10 μ J) are shown in Fig. 2. Unlike the static conditions of Newton's experiment, in our case the object is ultimately vaporized by the X-ray pulse and the object size changes in the brief interval that the pulse takes to reflect back to the particle, as depicted in Fig. 3. (The normal-incidence mirror is also locally destroyed by the pulse energy, but not before reflecting the pulse⁸.) We can describe our interference pattern as an X-ray hologram, caused by the interference of a reference beam scattered from the known sphere on the first pass, and then scattered again from the unknown exploding sphere on the second pass. This hologram encodes both the time delay and the structural change.

The delay time between the pumping and probing of the sphere by the FEL pulse depends on the distance l from the particles to the backing mirror, given simply as $\Delta t = 2l / c$, where c is the speed of light in a vacuum. We used both a wedge-shaped spacing between the particle-coated membrane and the backing multilayer X-ray mirror, and a stair-stepped mirror, producing values of l varying between 30 μm and 1200 μm , corresponding to delays between 200 fs and 8 ps.

There is no need to precisely measure the distance l , as this distance is encoded directly in the hologram. The geometry of the dusty-mirror hologram can be easily understood by unfolding the optical train and considering path lengths of rays scattering from two particles separated longitudinally by $2l$. For a scattering angle θ , the path difference of these scattered rays (for the approximation of a detector at infinity) is $2l(1 - \cos \theta) \approx l\theta^2$. In the forward direction ($\theta = 0$) rays will add constructively if the object does not change during the delay. Otherwise, if the optical path through the object does change during this interval, there will be a phase shift φ applied to the fringe pattern. Each bright ring of the hologram counts another wavelength of path difference, so at the N^{th} bright ring we have $l\theta^2 + \varphi\lambda / (2\pi) \approx N\lambda$, in agreement with Newton's observation when the object does not change ($\varphi = 0$). From a measurement of the angles of the bright rings we can derive l and hence the delay $2l/c$ to an accuracy of about 1 fs, and we can determine φ to an accuracy of 3° for delays less than 1 ps (see Methods).

We used this holographic set-up to investigate the explosion of spherical particles caused by a focused X-ray FEL pulse. We wish to study the dynamics of material in the extreme conditions of intense FEL pulses, both during the pulse and as it turns into a plasma. Models have been developed⁹⁻¹¹ to predict the effects of intense X-ray pulses on materials and particles¹², and to understand the resolution limitations of flash imaging^{3,12}, the technological limitations of X-ray optics⁸, and the fundamental physics

of light-matter interactions¹³. However, there has been no experimental validation of these models. Indeed, there have been no structural methods to follow early steps in plasma formation. Spherical particles are the simplest shape to consider for modelling the interaction dynamics and scattering of x-ray pulses, and they can be size selected to a very homogeneous distribution¹⁴ to give accurate scattering measurements. In these experiments we focused 32.5 nm wavelength pulses of energies between 2 and 18 μJ to about a 20- μm Gaussian-profiled spot on the sample¹⁵. The highest peak intensity was 10^{14} W/cm^2 , more than 5,000 times the damage threshold of the latex particles¹⁶.

Each hologram shown in Fig. 2 is the superposition of the time-delay holographic patterns of about 1000 quasi-identical latex spheres of diameter 140 nm, illuminated by the focused pulse. Since the FEL pulse is almost completely transversely coherent, the superposition from the many spheres occurs coherently, and we observe speckle across the hologram. Phase retrieval techniques¹⁷⁻¹⁹ could be used to reconstruct the positions of all the spheres. To examine the dynamics we compare our holographic measurements at different delay times to simulations based on the propagation of the pulse through the object and subsequent hydrodynamic explosion from the absorbed energy as shown in Fig. 4 (a)-(c) (see Methods). We observe that the hologram intensity envelope is unchanged for delays shorter than 1 ps (only the 0.5 ps curve is shown for these short delays) and becomes narrower with longer delays, indicating that the particle diameter begins to increase. As shown in Fig. 4 (d), this narrowing of the structure factor is observed for delays longer than 3.8 ps, in agreement with our simulations that predict the transverse particle diameter has increased by 40% (60 nm) at 3.8 ps.

At a delay of 500 fs, there is no observable change in the hologram intensity envelope, and we estimate that the spheres have not expanded by more than 20% of their transverse diameter, or 30 nm. We have, however, a more sensitive measure of

the structural change of the particle: the holographically-determined phase shift, φ . We observe an increase in φ with delay, for all but the lowest pulse fluences. This is shown in Fig. 4 (e), indicating a larger optical path length through the exploding object compared to the reference. Since at this wavelength the refractive index of latex is less than unity (equal to 0.87 at room temperature), this increase in optical path corresponds to a decrease in refracting material along the path as time progresses (or a change in refractive index towards unity). We can simulate the phase shift of the exploding spheres from our hydrodynamic model. This also shows an increase of φ with delay, primarily due to ball material expanding away in a transverse direction to the beam path (i.e. the projected mass is decreasing). A 6-nm expansion in diameter gives a calculated 5° phase shift, as observed at a 350 fs delay.

A further factor is a change in refractive index following the cooling of electrons that were ionised from the atoms during the initial (holographic reference) pulse. Our hydrodynamic model predicts that the peak electron temperature of the spheres reaches 10^5 K during the 10^{14} W/cm² pulse. Accurate calculations of refractive index for this degenerate “warm dense matter” regime¹³ are not available, and the observed phase shift could be due to a 1.5% increase in refractive index caused by the electron heating (the available models of high-temperature plasmas predict less than a 0.3% increase). The expansion of 6 ± 3 nm at 350 fs delay is thus considered an upper bound of the explosion. Extrapolating to the end of the pulse duration, we predict an explosion of no more than 0.4 nm during the pulse. Thus, it appears feasible to overcome conventional radiation damage limits⁴ in soft-X-ray microscopy of cells^{20,21} with sufficiently short and intense X-ray FEL pulses².

Time-delay holography, inspired by Newton’s experiment, provides a simple method to achieve extremely high spatial and temporal resolution in a single image. The method is well suited to a wide range of short-pulse X-ray sources²²⁻²⁴, and could

be extended to hard-X-ray pulsed sources using a grazing-incidence geometry as well as to high-resolution experiments using ultrafast optical pump pulses^{25,26}. The coherence demands of the experiment are relatively modest, as Newton's success attests. The advantage of the almost complete spatial coherence of the X-ray FEL pulses is that holographic reconstructions over large fields of view will be possible, allowing us to examine the time evolution of complex geometries, to study shocks and crack formation, ablation, melting, plasma formation, ultrafast phase transitions, and non-linear optical effects.

Methods Summary

Experiments were conducted at FLASH, the soft-X-ray FEL at DESY in Hamburg. The FEL pulses were focused to a 20- μm diameter beam on the dusty-mirror sample. The converging beam first passes through a hole in a flat mirror substrate that later reflects the scattered waves to interferometrically combine on a CCD detector. The dusty mirrors consisted of size-selected polystyrene spheres placed onto silicon wafers arrayed with openings supporting thin silicon nitride membranes. These were sandwiched against normal-incidence multilayer mirrors. We obtained a range of time delay distances for various positions across the wafer by either setting the wafer at a small wedge angle to the mirror or by stacking a staircase of mirrors. Single-pulse holograms were recorded at many positions across the wafer. Holograms were sorted according to the measured pulse fluence (which has a large pulse to pulse variation due to the FEL Self Amplification of Spontaneous Emission process⁷). From the fringe positions in the hologram we extracted the time delay to an accuracy of about 1 fs, and the change in forward-scattered particle phase shift to an accuracy of about 3° for delays shorter than 1 ps. We compared the phase shift and hologram intensity envelope, defined as the mean of curves fitted through the maximum and minimum fringe intensities, to calculations obtained from a radiation hydrodynamics model. The width

of the intensity envelope of the hologram depends inversely on the sphere width, so a narrowing of the envelope function indicates the sphere explosion.

Full Methods

Experiments were carried out at FLASH, the soft-X-ray FEL at DESY in Hamburg, under conditions previously reported³. Compared with previous work the diffraction camera was rotated by 180° to admit the focused incident beam onto the sample through the detector mirror hole. The detector accepts $\pm 15^\circ$, allowing a hologram resolution of 62 nm at 32.5 nm wavelength.

“Dusty mirror” samples. Polystyrene spheres (PostNova, Germany) were aerosolised by charge-reduction electrospray (TSI, model 3480), and selected with a differential mobility analyser (TSI, model 3936) to reduce the size distribution from 16% to less than 4% (as measured by soft-x-ray diffraction at the Advanced Light Source), prior to deposition onto the membrane¹⁴. The substrate, which had several etched openings or “windows” that were 1.5 mm square and which supported the freestanding 20-nm thick silicon nitride membrane, was manufactured at the Microfabrication Center at LLNL. This was then wedged against a single multilayer mirror or a stack of stepped mirrors, with the substrate’s nitride side facing the mirror. The mirror assemblies gave a range of distances l between the spheres and the mirror and we selected different delay times by exposing different windows in the substrate. We made assemblies for distances l from 30 μm to 1200 μm . The largest wedge angle of the nitride substrate was 0.6° , which gives a spread of 0.7 fs in delay over the 20 μm width of the beam. The sample backing multilayer mirror consisted of 50 Si/Mo/B₄C trilayers and was designed for a peak reflectivity of 50% under normal incidence at a wavelength of 32.5 nm. The peak reflectivity varied by less than 10% for an angle of incidence up to 15° . The pulse fluence was up to 50 times higher than the damage threshold of the backing mirror, and caused it to ablate, but not before the pulse was reflected⁸.

Holograms encode the delay time in the fringe pattern caused by the interference of the reference and object waves. Constructive interference occurs at scattering angles θ according to $2l(1 - \cos \theta) - 2l(1 - \cos \alpha) + \varphi \lambda / (2\pi) = N \lambda$, for path differences $N \lambda$ shorter than the coherence length, where φ is the phase shift of the object relative to the reference, α is the angle between the incident beam and mirror normal, and θ is the angle between the scattered beam and mirror normal. The above equation is fit to the measured θ values of the bright rings to determine the quantities l and φ . The angle α is determined from measurements with attenuated pulses (where damage to the sample does not occur and φ is zero) and was less than 0.8° for all mirror assemblies. The accuracy to which we determine l is limited by the precision to which we can measure θ , given by $\Delta l / l \approx 2 \Delta \theta / \theta$. Through fitting, we determine the radius of the interference maxima to better than 1/10 the width of a pixel at angles corresponding to 500 pixels on the CCD. This contribution to the error in l is therefore about 1 part in 2500, or 0.2 fs for a 500 fs delay. However, the sample to CCD distance is only known to 1 part in 500, which places a systematic error in the estimation of the angle θ , corresponding to a 1 fs temporal resolution on the 500 fs delay. This compares with an accuracy of less than 60 fs for state-of-the art timing diagnostics to synchronize an X-ray beam to a laser beam²⁷.

The determination of the phase shift is independent of the CCD distance. The accuracy for measuring φ depends on the number of pixels spanning an entire fringe, which is greatest at the centre of the pattern. However, the hole in our mirror prevents us from measuring the centre, so we determine the fringe shift for the observed fringes at $q < 5 \mu\text{m}^{-1}$ to estimate the phase shift at $q = 0$. We observe no dependence of phase shift on fringe number in this range, implying that the explosion is spherical over lengthscales larger than 200 nm. We determined φ to an accuracy of about 3° for delays shorter than 1 ps. At longer delays the error in φ increased in proportion to the delay, due to the decreasing fringe spacing with increasing delay. As in interferometry, higher

accuracy of the phase measurement could be obtained by measuring the fringes in smaller intervals.

There will be no interference for path differences $N \lambda$ greater than the coherence length, which can be no longer than the 7.5- μm FEL pulse length (or a maximum of 230 fringes). The measured fringe visibility also depends on the CCD pixel width. The fringe spacing decreases with N and intensity modulation is not observed when this spacing spans only a single pixel. In our measurements we have observed a maximum of about 150 fringes, limited by the pixel width. We define the hologram intensity envelope as the mean of curves fitted through the maximum and minimum fringe intensities, which is not dependent on the fringe visibility.

Hydrodynamic simulations. The light intensity distribution inside the polystyrene spheres was calculated using Mie theory²⁸; this time-independent model is applicable since the time for the light to propagate through the sphere (approximately 2 fs) is much shorter than the pulse length (25 fs). We based our estimate of the complex index of refraction on published room-temperature solid-density values²⁹, and corrected for changes with temperature and density using an average ion model employing screened hydrogen potentials³⁰. We calculated the temperature and density of the sphere using the HYDRA radiation hydrodynamics code³¹. This model accounts for radiation transport and electron thermal conduction. The change in transverse sphere diameter, ΔD , projected along the ray direction z , is quantified as

$$\Delta D / 2 = (2\pi / m) \int_{-\infty}^{\infty} \int_0^{\infty} r_{\perp}^2 \rho(r_{\perp}, z) dr_{\perp} dz, \text{ where } \rho \text{ is the sphere density, } m \text{ its mass, and } r_{\perp}$$

is the radial coordinate perpendicular to z . Finally, the superposition of the far-field diffraction patterns of the undamaged sphere and of the exploded sphere was calculated using the Fresnel-Kirchhoff diffraction integral³². This hologram is the product of the structure factors of the undamaged and damaged balls, modulated by the delay-encoding ring pattern. The width of the intensity envelope of the hologram depends inversely on

the sphere width, so a narrowing of the envelope function indicates the sphere explosion.

Author Information: The authors declare that they have no competing financial interests.

Correspondence and requests for materials should be addressed to H.N.C (henry.chapman@llnl.gov).

Author Contributions: H.N.C. conceived the experiment and H.N.C., S.P.H., A.B., S.M., B.W.W., S.B., M.F., R.A.L. and A.S. contributed to its design. S. Bajt, E.S., and H.N.C. designed the camera and designed and characterized the dusty mirror optics. Samples were prepared by M.J.B., W.H.B, and M.F. and characterized by M.J.B., S.M., S.B., and D.A.S. H.N.C., M.J.B., A.B., S.B., S.M., M.F., B.W.W., W.H.B., U.R., T.M., C.B., D.A.S., F.B., M.B., C.C, G.H., M.M.S, and J.H. carried out the experiment. M.K., R.T., and E.P. interfaced the experiment to FLASH and developed diagnostics. H.N.C., S.P.H., M.J.B. and M.B., carried out data analysis. All authors discussed the results and contributed to the final manuscript.

1. Newton, I. *Opticks* (originally published in London, 1704). New edition (Dover Publications, New York, 1952). Book 2, part IV.
2. Solem, J. C. & Baldwin, G. C. Microholography of living organisms. *Science* **218**, 229–235 (1982).
3. Chapman, H.N. *et al.* Femtosecond diffractive imaging with a soft-X-ray free-electron laser. *Nat. Phys.* **2**, 839–843 (2006).
4. Howells, M.R. *et al.* An assessment of the resolution limitation due to radiation-damage in x-ray diffraction microscopy. *J. Electron. Spectrosc. Relat. Phenom.* (in the press). Preprint at <<http://arxiv.org/abs/physics/0502059>> (2005).
5. Young, T. The Bakerian Lecture: On the theory of light and colours. *Phil. Trans. Roy. Soc.* **92**, 12-48 (1802) (Corollary III of Proposition VIII, p. 41)
6. de Witte, A.J. Interference in scattered light. *Am. J. Phys.* **35**, 301–313 (1967).

7. Ayvazyan, V. *et al.* First operation of a free-electron laser generating GW power radiation at 32 nm wavelength. *Eur. Phys. J. D* **37**, 297-303 (2006).
8. Hau-Riege, S. *et al.* Interaction of nanometer-scale multilayer structures with x-ray free-electron laser pulses. *Phys. Rev. Lett.* **98**, 145502 (2007).
9. Bergh M., Timneanu N. & van der Spoel, D. A model for the dynamics of a water cluster in a X-ray FEL beam. *Phys. Rev. E* **70**, 051904 (2004).
10. Jurek Z., Faigel G. & Tegze, M. Dynamics in a cluster under the influence of intense femtosecond hard X-ray pulses. *Eur. Phys. J. D* **29**, 217-229 (2004).
11. Hau-Riege, S.P., London, R.A. & Szöke, A. Dynamics of biological molecules irradiated by short x-ray pulses. *Phys. Rev. E* **69**, 051906 (2004).
12. Neutze, R., Wouts, R., van der Spoel, D., Weckert, E. & Hajdu, J. Potential for biomolecular imaging with femtosecond X-ray pulses, *Nature* **406**, 752-757 (2000).
13. Lee, R. *et al.* Finite temperature dense matter studies on next-generation light sources. *J. Opt. Soc. Am. B*, **20**, 770-778 (2003).
14. Bogan, M.J., Benner, W.H., Hau-Riege, S.P., Chapman, H.N. & Frank, M. Aerosol methods for x-ray diffractive imaging: Size-selected nanoparticles on silicon nitride foils. *J. Aer. Sci.* (2007), submitted.
15. Sorokin, A.A. *et al.* Method based on atomic photoionization for spot-size measurement on focused soft x-ray free-electron laser beams. *Appl. Phys. Lett.* **89**, 221114 (2006).
16. Gaur, U. & Wunderlich, B. Heat capacity and other thermodynamic properties of linear macromolecules. V. Polystyrene. *J. Phys. Chem. Ref. Data*, **11**, 313–325 (1982).
17. Fienup, J. R. Reconstruction of a complex-valued object from the modulus of its Fourier transform using a support constraint, *J. Opt. Soc. Am. A* **4**, 118–123 (1987).

18. Miao, J., Charalambous, P., Kirz, J. & Sayre, D. Extending the methodology of x-ray crystallography to allow imaging of micrometre-sized non-crystalline specimens. *Nature* **400**, 342–344 (1999).
19. Marchesini, S. *et al.* X-ray image reconstruction from a diffraction pattern alone. *Phys. Rev. B* **68**, 140101R, (2003).
20. Larabell, C. A. & Le Gros, M. A. X-ray Tomography Generates 3-D Reconstructions of the Yeast, *Saccharomyces cerevisiae*, at 60-nm Resolution. *Mol. Biol. Cell* **115**, 957–962 (2004).
21. Shapiro, D. *et al.* Biological imaging by soft x-ray diffraction microscopy. *Proc. Nat. Acad. Sci.* **102**, 15343–15346 (2005).
22. Bartels, R.A. *et al.* Generation of spatially coherent light at extreme ultraviolet wavelengths. *Science* **297**, 376-378 (2002).
23. Schoenlein, R. W. *et al.* Femtosecond X-ray Pulses at 0.4 Å Generated by 90° Thomson Scattering: A Tool for Probing the Structural Dynamics of Materials. *Science* **274**, 236-238 (1996).
24. Schoenlein, R. W. *et al.* Generation of Femtosecond Pulses of Synchrotron Radiation. *Science* **287**, 2237-2240 (2000).
25. Temnov, V.V., Sokolowski-Tinten, K., Zhou, P. & von der Linde D., Ultrafast imaging interferometry at femtosecond-laser-excited surfaces. *J. Opt. Soc. Am. B* **23**, 1954–1964, (2006).
26. Cavalleri, A. *et al.*, Femtosecond structural dynamics in VO₂ during an ultrafast solid-solid phase transition, *Phys. Rev. Lett.* **87**, 237401 (2001).
27. Cavalieri, A.L. *et al.* Clocking femtosecond x-rays. *Phys. Rev. Lett.*, **94**, 114801 (2005).

28. Bohren C.F. & Huffman, D.R. *Absorption and Scattering of Light by Small Particles*. Wiley-Interscience, New York (1983).
29. Henke, B.L., Gullikson, E.M. & Davis, J.C., X-ray interactions: photoabsorption, scattering, transmission, and reflection at $E=50-30000$ eV, $Z=1-92$. *Atom. Nucl. Data Tabl.* **54**, 181-342 (1993).
30. Zimmerman G.B. & More, R.M. Pressure ionization in laser-fusion target simulation. *J. Quant. Spectrosc. Radiat. Transf.* **23**, 517-522 (1980).
31. Marinak, M.M. *et al.* Three-dimensional HYDRA simulations of National Ignition Facility targets. *Phys. Plasmas.* **8**, 2275-2280 (2001).
32. Goodman, J.W. *Introduction to Fourier Optics*, McGraw-Hill, Boston (1996).

Acknowledgements Special thanks are due to the scientific and technical staff of FLASH at DESY, Hamburg, in particular to T. Tschentscher, S. Dusterer, J. Schneider, J. Feldhaus, R. L. Johnson, U. Hahn, T. Nuñez, K. Tiedtke, S. Toileikis, E. L. Saldin, E. A. Schneidmiller, and M. V. Yurkov. We also thank R. Lee, R. Falcone, M. Ahmed and T. Allison for discussions, J. Alameda, E. Gullikson, F. Dollar, T. McCarville, F. Weber, J. Crawford, C. Stockton, M. Haro, J. Robinson, H. Thomas, M. Hoener, and E. Eremina for technical help with these experiments. This work was supported by the following agencies: The U.S. Department of Energy (DOE) under contract to the University of California, Lawrence Livermore National Laboratory; The National Science Foundation Center for Biophotonics, University of California, Davis; The Advanced Light Source, Lawrence Berkeley Lab, under DOE contract; Natural Sciences and Engineering Research Council of Canada (NSERC Postdoctoral Fellowship to M.J.B); Swiss National Science Foundation (fellowship to U.R.); Sven and Lilly Lawskis Foundation (doctoral fellowship to M.M.S.); the U.S. Department of Energy Office of Science to the Stanford Linear Accelerator Center; the European Union (TUIXS); The Swedish Research Council; The Swedish Foundation for International Cooperation in Research and Higher Education; and The Swedish Foundation for Strategic Research.

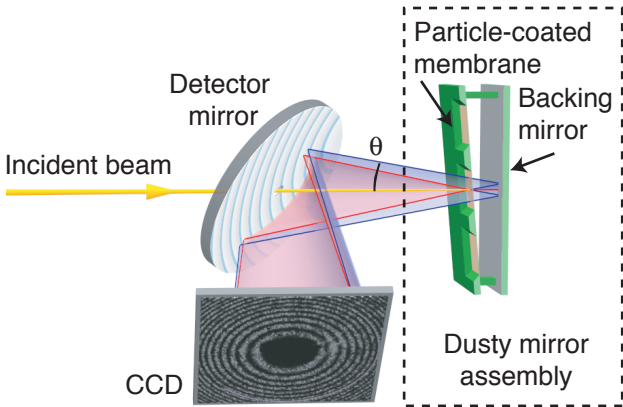
Figure 1. Schematic of the apparatus, similar to Newton’s dusty mirror experiment. The incident FEL pulse from the left passes through a hole in a multilayer-coated detector mirror. The “dusty mirror” consists of particles on a 20-nm thick silicon nitride membrane backed by a multilayer-coated plane mirror. This returns the direct beam back through the hole in the detector mirror, which reflects the diffracted light onto a CCD detector. The prompt diffraction (blue, the reference wave) and delayed diffraction (red, the object wave) interfere to generate the hologram on the CCD detector.

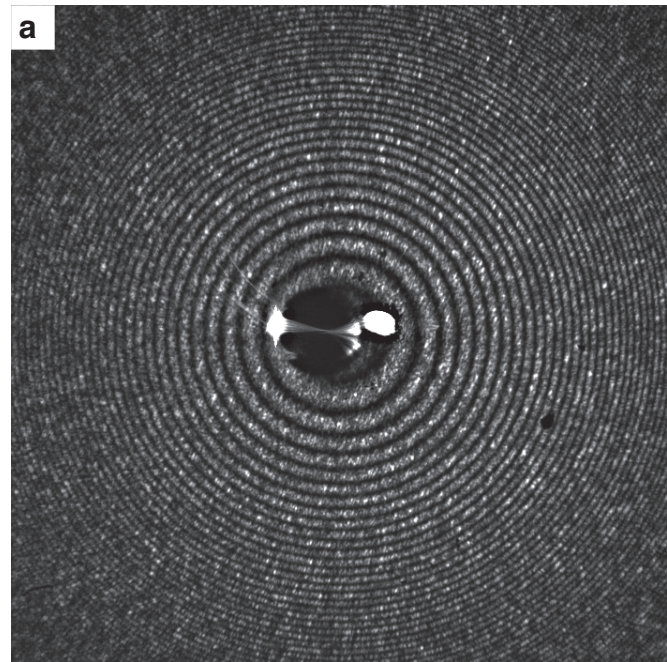
Figure 2. Time-delay X-ray holograms of 140-nm diameter polystyrene spheres. The time delays were (a) 348 ± 1 fs and (b) 733 ± 2 fs. The pulses were 32-nm wavelength, 25-fs duration with intensities $(0.5 \pm 0.2) \times 10^{14}$ W/cm². The intensities of the holograms are shown on a linear greyscale, to a half-width of $4.5 \mu\text{m}^{-1}$. We derive the time delays and the change in optical path through the exploding particles from the fringe pattern. The particle sizes are determined from the envelope of the intensity.

Figure 3. Geometry for time-delay holography. A pulse is incident (at an angle, for clarity) on a particle located a distance l from a mirror. (a) Time $t = 0$. (b) At time $t = l/c$ the pulse and prompt diffraction have reached the mirror. The pulse length is much less than l . (c) At time $t = 2l/c$ the pulse returns to the particle. By this time the particle has undergone changes due to the initial interaction. The mirror also explodes after it reflects the pulse, but this has no effect on the reflected pulse. (d) The delayed diffraction (red) co-propagates with the prompt diffraction (blue) and these waves interfere at the detector (not shown). (e) The geometry can be conceptually unfolded for easier analysis.

Figure 4. Determination of the explosion of polystyrene spheres. (a)–(c) Simulated density profile of an initially uniform 140-nm diameter polystyrene ball

(black circle) irradiated by a 25 fs, 10^{14} W/cm² soft-X-ray FEL pulse from the left, after 0.5, 0.9, and 3.2 ps. (d) Measured (red) and simulated (blue) envelope of the hologram intensity as a function of momentum transfer $q = (2 / \lambda) \sin(\theta / 2)$, for three pulse delays and pulse intensities of $(0.8 \pm 0.3) \times 10^{14}$ W/cm². The narrowing of the envelope with time indicates a larger particle diameter, in agreement with the simulations. (e) Average phase shifts, determined from 129 separate holograms measured at various delays and pulse intensities, as a function of delay. The phase shifts were averaged over ranges of time delay (denoted by the horizontal error bars) and ranges of pulse intensity (indicated by the symbol colour). Vertical error bars give one standard deviation in the phase shift. Solid lines guide the eye. Dashed lines are the phase shifts calculated from hydrodynamic simulations. The approximate change in the ball diameter (ΔD) as obtained from the model is shown on the right-hand axis.



a**b**